Letter

Gravitational waves from supermassive black hole binaries in light of the NANOGrav 15-year data

John Ellis,[1,2,3,*] Malcolm Fairbairn,[2,†] Gert Hütsi,[1,‡] Juhan Raidal,[1,§] Juan Urrutia,[1,4,‖] Ville Vaskonen,[1,5,6,¶] and Hardi Veermäe[1,**]

[1]*Keemilise ja Bioloogilise Füüsika Instituut, Rävala puiestee 10, 10143 Tallinn, Estonia*
[2]*Physics Department, King's College London, Strand, London, WC2R 2LS, United Kingdom*
[3]*Theoretical Physics Department, CERN, CH 1211 Geneva, Switzerland*
[4]*Department of Cybernetics, Tallinn University of Technology, Akadeemia tee 21, 12618 Tallinn, Estonia*
[5]*Dipartimento di Fisica e Astronomia, Università degli Studi di Padova, Via Marzolo 8, 35131 Padova, Italy*
[6]*Istituto Nazionale di Fisica Nucleare, Sezione di Padova, Via Marzolo 8, 35131 Padova, Italy*

(Received 12 July 2023; accepted 30 November 2023; published 10 January 2024)

The NANOGrav and other pulsar timing arrays (PTAs) have recently announced evidence for nHz gravitational waves (GWs) that may originate from supermassive black hole (SMBH) binaries. The spectral index of the GW signal differs from that predicted for binary evolution by GW emission alone, and we show that environmental effects such as dynamical friction with gas, stars, and dark matter improve the consistency of the SMBH binary model with the PTA data. We comment on the possible implications of environmental effects for PTA observations of fluctuations in the GW frequency spectrum and measurements of GWs at higher frequencies.

DOI: 10.1103/PhysRevD.109.L021302

Introduction. Several ongoing pulsar timing array (PTA) projects—the North American Nanohertz Observatory for Gravitational Waves (NANOGrav), the European PTA, the Parkes PTA, and the Chinese PTA—have recently released their latest data [1–4]. Most importantly, the NANOGrav Collaboration has found evidence [5] in NANOGrav 15-year (NG15) data for the Hellings-Downs quadrupolar correlation [6] (see also [4,7,8])—a key characteristic of gravitational waves (GWs)—in the common-spectrum process observed previously by them [9] and other PTAs [10–12]. This is a landmark in GW astronomy, of significance comparable to the first indirect detection of GWs emitted by binary pulsars [13] and the first direct observation of GW emissions from stellar-mass black hole (BH) binaries [14]. This discovery of a nHz stochastic GW background opens a new window on astrophysical processes that were previously unobserved. We assume here that the origin of the PTA signal is a population of supermassive black hole (SMBH) binaries (see also [15,16]) and explore the astrophysical implications of this possibility.[1]

Accretion around SMBHs drives active galactic nuclei (AGNs) and is thought to play a role in the formation of SMBH binaries [59,60]. At an early stage, the binary evolution is driven by dynamical friction with gas, stars, and dark matter [61]. However, a prerequisite for SMBH mergers is the formation of tightly bound binaries that can radiate GWs efficiently. It is not yet understood how this stage of SMBH binary evolution is reached, an issue commonly known as the "final parsec problem" [61]. If the binaries can overcome it, an important source of evolution at subparsec scales is energy loss via GW emission until it is the main driver of the evolution close to merging. SMBH binaries driven only by GW emission are naively expected to produce an almost flat background with a spectral index $\gamma = 13/3$ [62]. The recent NG15 data [5] on GWs, although compatible with this value at the 99% CL, prefer a lower value of γ. This hints that the GWs may be emitted by SMBH binaries that are experiencing additional energy loss via environmental effects, which

*john.ellis@cern.ch
†malcolm.fairbairn@kcl.ac.uk
‡gert.hutsi@kbfi.ee
§juhan.raidal@student.manchester.ac.uk
‖juan.urrutia@kbfi.ee
¶ville.vaskonen@pd.infn.it
**hardi.veermae@cern.ch

[1]Numerous interpretations of the NANOGrav 12.5-year data [9] based on cosmological sources have been put forward, including cosmic strings and domain walls [17–27], first-order phase transitions [28–37], and primordial fluctuations [38–57]. Many of these models with a spectral slope $\gamma > 13/3$ are disfavored by the current data [58], for instance, cosmic strings or primordial black hole seeds for SMBHs.

might be related to whatever dynamics overcomes the final parsec problem.

In this Letter, we follow [63] in using the extended Press-Schechter (EPS) formalism to estimate the SMBH binary formation and merger rates. We go beyond [63] by including scatter in the SMBH-halo mass relation and by modifying the evolution of the SMBH binaries to include energy loss via environmental effects as well as GWs. Our analysis improves existing SMBH interpretations [15] of the NG15 data by accurately modeling the long-tailed statistical fluctuations in the GW spectrum without relying on Gaussian approximations. We find that the best fit to the NG15 data [5] is given by a phenomenological model of SMBH binary evolution that includes environmental energy loss, with a log-likelihood difference of 10 compared to purely GW-driven evolution, and hence is favored by more than 2σ. Within this framework, we find that the efficiency for the production of SMBH mergers $p_{\rm BH}$ is probably quite high and close to the maximal allowed value. These results provide important constraints on astrophysical scenarios for the interlinked dynamics of SMBHs and their host galaxies, and suggest promising rates for observing mergers of lower-mass BHs in detectors sensitive to GWs with higher frequencies.

SMBH background with environmental effects. The mean of the GW energy density spectrum generated by a population of SMBH binaries can be estimated as [62]

$$\Omega_{\rm GW}(f) \equiv \frac{1}{\rho_{\rm c}}\frac{{\rm d}\rho_{\rm GW}}{{\rm d}\,\ln f} = \frac{1}{\rho_{\rm c}}\int {\rm d}\lambda \frac{1+z}{4\pi D_L^2}\frac{{\rm d}E_{\rm GW}}{{\rm d}\,\ln f_r}, \quad (1)$$

where D_L denotes the source luminosity distance, ${\rm d}E_{\rm GW}/{\rm d}\,\ln f_r$ gives the energy emitted by the source per logarithmic frequency interval, and $f_r \equiv (1+z)f$ denotes the frequency in the source frame, i.e., at the time of emission. The differential BH merger rate in the observer frame is

$${\rm d}\lambda = {\rm d}\mathcal{M}{\rm d}\eta{\rm d}z\frac{1}{1+z}\frac{{\rm d}V_c}{{\rm d}z}\frac{{\rm d}R_{\rm BH}}{{\rm d}\mathcal{M}{\rm d}\eta}, \quad (2)$$

where $\mathcal{M}$ denotes the binary chirp mass, η its symmetric mass ratio, V_c the comoving volume, and $R_{\rm BH}$ the comoving BH merger rate density. It is given by

$$\frac{{\rm d}R_{\rm BH}}{{\rm d}m_1{\rm d}m_2} = p_{\rm BH}(m_1,m_2,z)\int {\rm d}M_1{\rm d}M_2\frac{{\rm d}R_h}{{\rm d}M_1{\rm d}M_2} \times p_{\rm occ}(m_1|M_1,z)p_{\rm occ}(m_2|M_2,z), \quad (3)$$

where $m_{1,2}$ are the masses of the merging BHs, $M_{1,2}$ are the masses of their host halos, R_h is the halo merger rate that we estimate with the EPS formalism [64–66], and $p_{\rm BH} \leq 1$ combines the SMBH occupation fraction in galaxies with the efficiency for the BHs to merge following the merging of their host halos. For simplicity, we assume a constant value for $p_{\rm BH}$, which we treat as a free parameter to be determined by fitting the NG15 data. As the GW background arises from a relatively narrow range of SMBH masses and redshifts, we expect that extending the parametrization by letting $p_{\rm BH}$ vary would have a minor effect on our conclusions. The halo mass-SMBH mass relation is encoded in $p_{\rm occ}$ that is the probability distribution of the SMBH mass.[2] We model the spread in the mass relation with a log-normal distribution:

$$p_{\rm occ}(m|M,z) = \frac{1}{\sqrt{2\pi}m\sigma}\exp\left[-\frac{\ln(m/\bar{m})^2}{2\sigma^2}\right] \quad (4)$$

with $\log_{10}(\bar{m}/M_\odot) = 8.95 + 1.4\log_{10}(M_*/10^{11}M_\odot)$ and $\sigma = 1.1$ following the fit to observations of inactive galaxies in [67,68], and relate the stellar mass M_* to the halo mass $M_{\rm halo}$ using the fit provided in [69]. The effect of using the fit to AGN and not including the scatter is discussed in the Supplementary Material [70].

The GW spectrum from an inspiraling binary is determined by its orbital evolution, and following NANOGrav [5] we assume circular binaries. The eccentricity of the orbits (considered, e.g., in [78]) would affect the GW spectrum by introducing higher harmonics, increasing the total power emitted in GWs, and modifying the frequency spectral index [79]. However, big eccentricities $e > 0.9$ would lead to an attenuation of the background due to the acceleration of the binary inspiral [80].

The binary may lose energy through a combination of GW emission and dissipative environmental effects:

$$\dot{E} = -\dot{E}_{\rm GW} - \dot{E}_{\rm env}, \quad (5)$$

where the dot denotes differentiation with respect to time. This energy loss causes orbital decay and growth in the orbital frequency. SMBH binaries are thought to go through several stages as they harden, starting with dynamical friction, followed by hardening due to close stellar encounters with stars populating the so-called "loss-cone" orbits [81], and finally, dissipation caused by viscous drag due to circumbinary gas disks [61]. The crossing of the final parsec is determined mostly by these last two effects, with the latter being the dissipation mechanism that is commonly thought to remain active after the GW emission has become significant (see, e.g., [82–84]), thus leading to faster binary hardening compared to the GW-only case.

The impact of the gas is not fully established; e.g., [85,86] argue that accretion from circumbinary disks might have quite the opposite effect; instead of hardening the binary, it might lead to the expansion of the orbit. More recent work predicts, however, inspiraling for more realistic cooler, thinner disks [87], nonzero eccentricities [88], and unequal masses [89]. Any slowing of the infall of binaries contributing in the low-frequency bins would worsen the

[2]Compared to Eq. (5) of Ref. [63], the normalization of $p_{\rm occ}$ is absorbed into $p_{\rm BH}$.

SMBH fit, whereas extra dissipation improves it, as we show below.

The characteristic timescales for the above processes are

$$t_{\rm GW} \equiv |E|/\dot{E}_{\rm GW} = 4\tau, \qquad t_{\rm env} \equiv |E|/\dot{E}_{\rm env}, \tag{6}$$

where $\tau = (5/256)(\pi f_r)^{-8/3}\mathcal{M}^{-5/3}$ denotes the coalescence time of the binary assuming GW emission alone. The effective timescale for the binary evolution is then $t_{\rm eff}^{-1} = t_{\rm GW}^{-1} + t_{\rm env}^{-1}$. Since the binding energy of the binary is $E = -(\pi f_r)^{2/3}\mathcal{M}^{5/3}/2$, where f_r is the frequency of the emitted GW, it follows that

$$\frac{{\rm d}\ln f_r}{{\rm d}t} = \frac{3}{2}t_{\rm GW}^{-1}\left(1 + \frac{t_{\rm GW}}{t_{\rm env}}\right), \tag{7}$$

and thus,

$$\frac{{\rm d}E_{\rm GW}}{{\rm d}\ln f_r} = \frac{{\rm d}E_{\rm GW}}{{\rm d}t}\frac{{\rm d}t}{{\rm d}\ln f_r} = \frac{1}{3}\frac{(\pi f_r)^{\frac{2}{3}}\mathcal{M}^{\frac{5}{3}}}{1 + t_{\rm GW}/t_{\rm env}}. \tag{8}$$

When $t_{\rm GW} \ll t_{\rm env}$, we obtain the usual spectrum for GW-driven coalescence. As the PTAs observe only a narrow range of frequencies, environmentally driven decay can be approximated by

$$\frac{t_{\rm env}}{t_{\rm GW}} = \left(\frac{f_r}{f_{\rm GW}}\right)^{\alpha_1 + \alpha_2 \ln f_r/f_{\rm GW} + \ldots}, \tag{9}$$

where $f_{\rm GW}$ denotes a reference frequency above which GW emission becomes dominant, and α_n are coefficients series expansion of $\ln t_{\rm env}/t_{\rm GW}$ in $\ln f_r$. At leading order, we can drop $\alpha_{n>1}$ terms and define $\alpha_1 \equiv \alpha$, so that the environmental effects are parametrized by a power-law dependence on the orbital frequency (cf. [90–93]) and choose[3]

$$f_{\rm GW}(\mathcal{M}, \eta, z) = f_{\rm ref}\left(\frac{\mathcal{M}}{10^9 M_\odot}\right)^{-\beta}, \tag{10}$$

where $f_{\rm ref}, \alpha > 0$ are phenomenological parameters that we constrain with the NG15 data (we note that $t_{\rm env}$ increases with f_r if $\alpha > 8/3$). Depending on the environmental mechanism for orbital decay, the range $\beta = 0.2$–0.8 has been considered in the literature [90,91,93]. Following Ref. [93], we fix $\beta = 0.4$. As the signal is generated by binaries in a relatively narrow BH mass range, we expect our results to be only weakly dependent on β.

Analysis. As reported by NANOGrav, a power-law fit of the form $\Omega_{\rm GW} = A(f/f_{\rm yr})^{5-\gamma}$ excludes the $\gamma = 13/3$ scaling naively expected for a background of SMBH binaries whose evolution is driven by GW emission at the 95% CL.[4] However, as shown in Fig. 1, due to the stochastic nature of the signal, the power law fails to capture many of its properties, and it could differ significantly from any one particular realization of the background. Moreover, due to the environmental effects, even the mean GW background is not a simple power law. Therefore, we use the full information provided in [5] for the probability distribution functions at each frequency bin $P_{\rm data}(\Omega, f_i)$ represented by the orange "violins" in Fig. 6 of Supplementary Material [70].

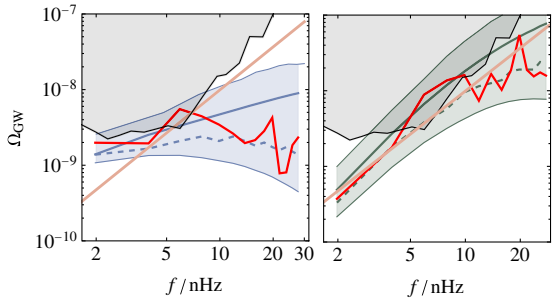

FIG. 1. The best-fit GW energy density for GW-driven binaries (left) and GW and environmentally driven effects (right), compared to the best power-law fit to the NG15 data (orange). The mean energy densities (1) are shown as full lines, and the most probable values as dashed lines, and in each case one random realization is shown in red and the 95% CL ranges are shaded. The gray curve shows the NG15 upper limit on signals from individually resolvable binaries [94].

Following [63], we generate Monte Carlo realizations of the stochastic GW background using the same frequency binning as the NANOGrav Collaboration, f_i. A realization of the SMBH background in a specific frequency bin is given by

$$\Omega_{\rm GW}(f_j) = \frac{1}{\ln(f_{j+1}/f_j)}\sum_{k=1}^{N(f_j)}\Omega_{\rm GW}^{(1)}(\vec{\theta}_b^k), \tag{11}$$

where $\vec{\theta}_b \equiv \{\mathcal{M}, z, \eta, f\}$ denotes the parameters of a binary, and $N(f_j)$ is drawn from a Poisson distribution determined by the expected number of binaries $\bar{N}(f_j) = \int_{f\in(f_j,f_{j+1})}{\rm d}\lambda{\rm d}\tau$ contributing to each bin. The contribution from an individual binary emitting at some frequency is

$$\Omega_{\rm GW}^{(1)}(f, \vec{\theta}_b) = \frac{1+z}{4\pi D_L^2 \rho_c}\frac{{\rm d}E_{\rm GW}}{{\rm d}t}. \tag{12}$$

To decrease the computation time, rather than generating realizations of the binary population, we instead generate values of $\Omega_{\rm GW}(f_j)$ directly. Assuming that there are no correlations between the frequency bins, i.e., no binaries cross between bins during the period of observation, the

[3]This parametrization of the environmental effects does not account for the ratio between the masses of the components of the binary. However, the majority of the binaries are expected to have mass ratios close to unity [63]. An analogous power-law model was used in the NANOGrav analysis [5].

[4]As a consistency check, we repeated our analysis for a power-law ansatz and reproduced the posteriors reported by NANOGrav [5].

statistical properties of $\Omega_{\rm GW}(f)$ can be inferred from the distribution of $\Omega^{(1)}_{\rm GW}(f,\vec{\theta}_b)$, which is given by[5]

$$P^{(1)}(\Omega|f,\vec{\theta}_f) \propto \int {\rm d}\lambda \left|\frac{{\rm d}t}{{\rm d}\ln f_r}\right| \delta(\Omega - \Omega^{(1)}_{\rm GW}), \quad (13)$$

and depends only on the parameters of the merger rate and binary evolution $\vec{\theta}_f = (p_{\rm BH}, \alpha, \beta, f_{\rm ref})$.

Finally, the distribution $P(\Omega|f_j,\vec{\theta}_f)$ of the total GW energy density (11) in each bin is estimated by dividing the signal into two pieces: the signal from the strongest sources and the rest (see the Supplementary Material [70] for details). The first component is modeled using a Monte Carlo approach simulating 4×10^5 realizations of the signal from these strong sources using single event distributions (13). The rest of the signal follows a narrow Gaussian distribution and can be simply modeled by its average. The probability distribution of $\Omega_{\rm GW}(f_j)$ possesses a long tail which it inherits from $P^{(1)}$.[6] Such long tails are expensive to resolve with the Monte Carlo approach, so we use $P^{(1)}$ to construct the large Ω tail analytically. This improves the statistical modeling of $\Omega_{\rm GW}(f_j)$ at large amplitudes for which a single source is expected to dominate the signal. We represent the probability distributions of Ω with and without the environmental effects for the best-fit parameter values in Fig. 6 of Supplementary Material [70] by the green and blue violins.

Our approach provides an accurate and fast[7] way of resolving the distribution $P(\Omega|f_j,\vec{\theta}_f)$ of spectral fluctuations in each frequency bin. This makes it feasible to perform accurate scans over a wide range of model parameters $\vec{\theta}_f$, and is thus a step forward from earlier analyses that relied on Gaussian process interpolation for SMBH population synthesis [15] or a relatively small number of realizations of the full SMBH population [78].

The likelihood of a given model $\vec{\theta}_f$ is

$$l(f_i|\vec{\theta}_f) \propto \prod_i \int {\rm d}\Omega\, P_{\rm data}(f_i|\Omega) P(\Omega|f_i,\vec{\theta}_f), \quad (14)$$

where the effective number of variables of $\vec{\theta}_f$ depends on the hypothesis made for the population: If the energy loss due to GW emission dominates—corresponding to very slow environmental energy loss $(t_{\rm env}\to\infty)$—the only parameter is $p_{\rm BH}$, whereas environmental energy loss is characterized by two additional parameters, $f_{\rm ref}$ and α. Finally, to compare the fits, we define the likelihood ratio

$$\ell_{\rm max} = \frac{\max_{\vec{\theta}_f} l(\vec{\theta}_f|H_1)}{\max_{\vec{\theta}_f} l(\vec{\theta}_f|H_2)}. \quad (15)$$

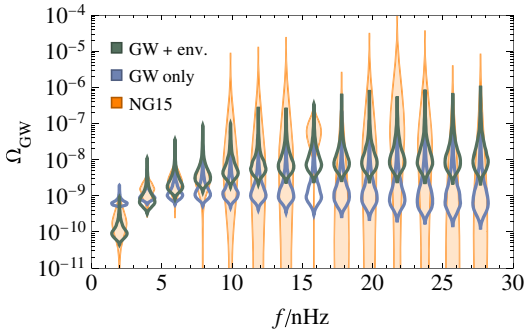

FIG. 2. The NG15 data on the energy density of GWs $\Omega_{\rm GW}$ (shown in orange) compared with the best fit assuming energy loss by GWs only (shown in blue), and the best fit including also energy loss by the environmental effects (shown in green). The posteriors for the parameters of the fits are shown in Fig. 3.

Results. We see in Fig. 2 that the NG15 data (shown in orange) are better fitted by the model including environmental effects (shown in green) than by the model where binaries evolve purely by emitting GWs (shown in blue). In particular, the fit including environmental energy loss captures better the dip in the lowest frequency bin at $f = 2$ nHz, whereas the GW-driven model has to balance the tilt by lowering the overall merging efficiency. We note that suppression of the signal at low frequencies is expected also when the binaries are eccentric [95].

We find that the best-fit value of the merging efficiency in the case of purely GW-driven binaries is $p_{\rm BH} = 0.07^{+0.05}_{-0.07}$, where the uncertainties are reported at the 68% CL. For the model including environmental effects, the fit prefers largervalues of $p_{\rm BH}$. In this case, we show in Fig. 3 the two-dimensional marginalized projections of the three-dimensional parameter space featuring the 68%, 95%, and 99% CL regions with different shades of green and the best fit as a white dot. The marginalized distributions of the three parameters are also shown. The best-fit values are $p_{\rm BH} = 0.84$, $\alpha = 2.0$, and $f_{\rm ref} \simeq 34$ nHz. We note, however, that there are significant correlations between the parameters, and the marginalized probability distributions are broad and asymmetric. The preferred value of α is consistent with previous model estimates and the value $\alpha = 8/3$ for which $t_{\rm env}$ would be frequency independent. The central value of $f_{\rm ref}$ corresponds to the apparent break in the spectral index seen in Fig. 6 of Supplementary Material [70].

The model that includes environmental effects gives a larger best-fit likelihood but also has more parameters, namely, $(p_{\rm BH}, \alpha, f_{\rm ref})$. The likelihood ratio with respect to the best fit for the purely GW-driven binaries (i.e., the limit

[5]The binary inclination can be exactly accounted for by including the inclination-angle-dependent prefactor in $\Omega^{(1)}_{\rm GW}$ and integrating over the inclination angle in $P^{(1)}$. We have checked that including the inclination angle in $P^{(1)}$ has a negligible effect, and thus we use the inclination angle averaged $\Omega^{(1)}_{\rm GW}$.

[6]It asymptotes to $P(\Omega|f,\vec{\theta}_f) \sim \Omega^{-\frac{5}{2}}$ as $\Omega\to\infty$, thus implying a divergent variance [63].

[7]It takes $\mathcal{O}(1)$ seconds per bin to compute $P(\Omega|f_j,\vec{\theta}_f)$ on an Apple M1 Pro 8-core processor.

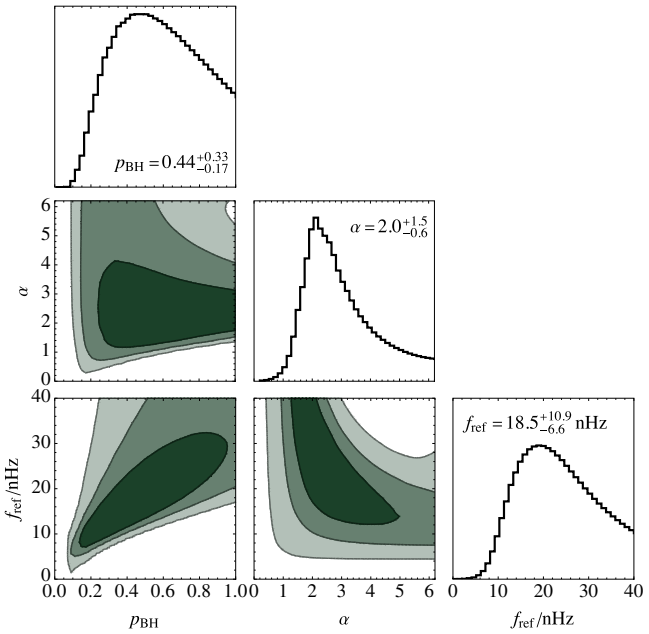

FIG. 3. Fit of the SMBH binary model with environmental effects parametrized by $f_{\rm ref}$, α, and $p_{\rm BH}$ to the NG15 data [5], for $\beta = 2/5$.

$f_{\rm ref} \to 0$) corresponds to $\Delta\chi^2 \sim -2 \log \ell_{\rm max} = 11$. In a Gaussian approximation, since the difference in the number of degrees of freedom between the hypotheses is 2, the model including environmental effects is favored over the model with pure GW evolution at the 2σ CL.

We note that the lower bound on $\Omega_{\rm GW}$ in the eighth bin at $f = 16$ nHz is relatively high. Large upward fluctuations are a feature of the long-tailed distribution of the GW spectra from SMBHs [63] and are not penalized heavily in a likelihood analysis. Relatively nearby SMBH binaries can generate such peaks. Specifically, the best fits for the GW-only and GW + environment models shown in Fig. 1 predict that 0.44 and 0.85 SMBH binaries are expected to be resolved with the current NANOGrav sensitivity, respectively. Intriguingly, we find that in both cases the individually resolvable binaries are most likely to be found in the 4–7 nHz frequency range, which coincides with a potential monochromatic GW signal seen by NANOGrav [94] and EPTA [96].

Discussion. The PTA results open an exciting new way to probe the environments of SMBH binaries. We show in Fig. 4 the effective timescales for the evolution of the binaries that best fit the NG15 data. We see that at the smallest radii, the binaries evolve by emitting GWs, whereas at larger distances the binary timescales are close to being flat. This suggests that at these distances the main mechanism driving binary evolution is viscous drag. Simulations show that in this regime the combination with other effects, e.g., loss-cone scattering as well as GW emission, leads to a distribution that is close to flat,

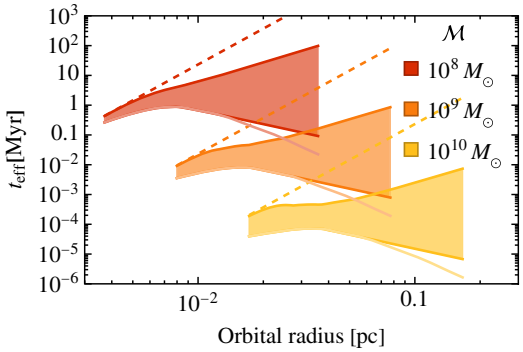

FIG. 4. Effective timescales $t_{\rm eff}$ for fits to the NG15 data shown as functions of the separations at which binaries are emitting GWs in the NANOGrav band (1–30 nHz), and for chirp masses $\mathcal{M} \in (10^8, 10^{10}) M_\odot$, which is the range found in [63] to dominate the stochastic GW background. The dashed lines are for energy loss by GWs alone, and the shaded regions are those favored at the 68% CL for a combination of energy loss by environmental effects and GWs. The two lower lines are computed with $\alpha < 4$ and $\alpha < 6$ as priors.

although the uncertainties are large. In general, we find that the phenomenological fit is consistent with the expected evolution of binaries in galactic environments.

As discussed in [63], although there are large uncertainties, extrapolation of the model predicts that GWs from mergers of lower-mass BHs should be observable in the higher frequency ranges where the LISA mission [97] and proposed atom interferometers such as AION [98] and AEDGE [99] are most sensitive, as well as other projects targeting the dHz frequency band [100,101]. LISA would be most sensitive to mergers of BHs with masses $(10^3, 10^7) M_\odot$ and AEDGE to the $(10^2, 10^5) M_\odot$ mass range. Observations of binaries of such intermediate-mass BHs could cast light on the mechanism for the assembly of SMBHs as well as probe strong gravity in a range beyond the reach of terrestrial laser interferometers. To the extent that the results of this Letter suggest a high merger efficiency $p_{\rm BH} \sim 0.5$, the merger rates might be greater than was estimated in [63], improving the prospects for seeing inspiraling intermediate-mass BH binaries by LISA and AEDGE to $\mathcal{O}(10^3)$ and by km-scale terrestrial atom interferometers to $\mathcal{O}(10)$.

Acknowledgments. The work of G. H., V. V., and H. V. was supported by European Regional Development Fund through the Center of Excellence program Grant No. TK133 and by the Estonian Research Council Grants No. PSG869 and No. PRG803. The work of J. E. and M. F. was supported by the United Kingdom STFC Grants No. ST/T000759/1 and No. ST/T00679X/1. The work of V. V. was partially supported by the European Union's Horizon Europe research and innovation program under the Marie Skłodowska-Curie Grant Agreement No. 101065736.

[1] G. Agazie *et al.* (NANOGrav Collaboration), Astrophys. J. Lett. **951**, L9 (2023).
[2] J. Antoniadis *et al.* (EPTA Collaboration), Astron. Astrophys. **678**, A48 (2023).
[3] A. Zic *et al.* (Parkes Pulsar Timing Array Collaboration), arXiv:2306.16230.
[4] H. Xu *et al.* (Chinese Pulsar Timing Array Collaboration), Res. Astron. Astrophys. **23**, 075024 (2023).
[5] G. Agazie *et al.* (NANOGrav Collaboration), Astrophys. J. Lett. **951**, L8 (2023).
[6] R. W. Hellings and G. S. Downs, Astrophys. J. Lett. **265**, L39 (1983).
[7] J. Antoniadis *et al.* (European Pulsar Timing Array Collaboration), Astron. Astrophys. **678**, A50 (2023).
[8] D. J. Reardon *et al.*, Astrophys. J. Lett. **951**, L6 (2023).
[9] Z. Arzoumanian *et al.* (NANOGrav Collaboration), Astrophys. J. Lett. **905**, L34 (2020).
[10] B. Goncharov *et al.* (Parkes Pulsar Timing Array Collaboration), Astrophys. J. Lett. **917**, L19 (2021).
[11] S. Chen *et al.* (European Pulsar Timing Array Collaboration), Mon. Not. R. Astron. Soc. **508**, 4970 (2021).
[12] J. Antoniadis *et al.* (International Pulsar Timing Array Collaboration), Mon. Not. R. Astron. Soc. **510**, 4873 (2022).
[13] R. A. Hulse and J. H. Taylor, Astrophys. J. Lett. **195**, L51 (1975).
[14] B. P. Abbott *et al.* (LIGO Scientific and Virgo Collaborations), Phys. Rev. Lett. **116**, 061102 (2016).
[15] G. Agazie *et al.* (NANOGrav Collaboration), Astrophys. J. Lett. **952**, L37 (2023).
[16] J. Antoniadis *et al.* (European Pulsar Timing Array Collaboration), arXiv:2306.16227.
[17] J. Ellis and M. Lewicki, Phys. Rev. Lett. **126**, 041304 (2021).
[18] S. Datta, A. Ghosal, and R. Samanta, J. Cosmol. Astropart. Phys. 08 (2021) 021.
[19] R. Samanta and S. Datta, J. High Energy Phys. 05 (2021) 211.
[20] W. Buchmuller, V. Domcke, and K. Schmitz, Phys. Lett. B **811**, 135914 (2020).
[21] S. Blasi, V. Brdar, and K. Schmitz, Phys. Rev. Lett. **126**, 041305 (2021).
[22] W. Buchmuller, V. Domcke, and K. Schmitz, J. Cosmol. Astropart. Phys. 12 (2021) 006.
[23] J. J. Blanco-Pillado, K. D. Olum, and J. M. Wachter, Phys. Rev. D **103**, 103512 (2021).
[24] R. Z. Ferreira, A. Notari, O. Pujolas, and F. Rompineve, J. Cosmol. Astropart. Phys. 02 (**2023**) 001.
[25] H. An and C. Yang, arXiv:2304.02361.
[26] Z.-Y. Qiu and Z.-H. Yu, Chin. Phys. C **47**, 085104 (2023).
[27] Z.-M. Zeng, J. Liu, and Z.-K. Guo, Phys. Rev. D **108**, 063005 (2023).
[28] Z. Arzoumanian *et al.* (NANOGrav Collaboration), Phys. Rev. Lett. **127**, 251302 (2021).
[29] X. Xue *et al.*, Phys. Rev. Lett. **127**, 251303 (2021).
[30] Y. Nakai, M. Suzuki, F. Takahashi, and M. Yamada, Phys. Lett. B **816**, 136238 (2021).
[31] P. Di Bari, D. Marfatia, and Y.-L. Zhou, J. High Energy Phys. 10 (2021) 193.
[32] A. S. Sakharov, Y. N. Eroshenko, and S. G. Rubin, Phys. Rev. D **104**, 043005 (2021).
[33] S.-L. Li, L. Shao, P. Wu, and H. Yu, Phys. Rev. D **104**, 043510 (2021).
[34] A. Ashoorioon, K. Rezazadeh, and A. Rostami, Phys. Lett. B **835**, 137542 (2022).
[35] M. Benetti, L. L. Graef, and S. Vagnozzi, Phys. Rev. D **105**, 043520 (2022).
[36] J. Barir, M. Geller, C. Sun, and T. Volansky, arXiv:2203.00693.
[37] M. Hindmarsh and J. Kume, J. Cosmol. Astropart. Phys. 04 (2023) 045.
[38] V. Vaskonen and H. Veermäe, Phys. Rev. Lett. **126**, 051303 (2021).
[39] V. De Luca, G. Franciolini, and A. Riotto, Phys. Rev. Lett. **126**, 041303 (2021).
[40] N. Bhaumik and R. K. Jain, Phys. Rev. D **104**, 023531 (2021).
[41] K. Inomata, M. Kawasaki, K. Mukaida, and T. T. Yanagida, Phys. Rev. Lett. **126**, 131301 (2021).
[42] K. Kohri and T. Terada, Phys. Lett. B **813**, 136040 (2021).
[43] G. Domènech and S. Pi, Sci. China Phys. Mech. Astron. **65**, 230411 (2022).
[44] S. Vagnozzi, Mon. Not. R. Astron. Soc. **502**, L11 (2021).
[45] R. Namba and M. Suzuki, Phys. Rev. D **102**, 123527 (2020).
[46] S. Sugiyama, V. Takhistov, E. Vitagliano, A. Kusenko, M. Sasaki, and M. Takada, Phys. Lett. B **814**, 136097 (2021).
[47] Z. Zhou, J. Jiang, Y.-F. Cai, M. Sasaki, and S. Pi, Phys. Rev. D **102**, 103527 (2020).
[48] J. Lin, S. Gao, Y. Gong, Y. Lu, Z. Wang, and F. Zhang, Phys. Rev. D **107**, 043517 (2023).
[49] K. Rezazadeh, Z. Teimoori, S. Karimi, and K. Karami, Eur. Phys. J. C **82**, 758 (2022).
[50] M. Kawasaki and H. Nakatsuka, J. Cosmol. Astropart. Phys. 05 (2021) 023.
[51] W. Ahmed, M. Junaid, and U. Zubair, Nucl. Phys. **B984**, 115968 (2022).
[52] Z. Yi and Q. Fei, Eur. Phys. J. C **83**, 82 (2023).
[53] Z. Yi, J. Cosmol. Astropart. Phys. 03 (2023) 048.
[54] V. Dandoy, V. Domcke, and F. Rompineve, SciPost Phys. Core **6**, 060 (2023).
[55] J.-X. Zhao, X.-H. Liu, and N. Li, Phys. Rev. D **107**, 043515 (2023).
[56] G. Ferrante, G. Franciolini, A. Iovino Junior, and A. Urbano, arXiv:2305.13382.
[57] Y. Cai, M. Zhu, and Y.-S. Piao, arXiv:2305.10933.
[58] A. Afzal *et al.* (NANOGrav Collaboration), Astrophys. J. Lett. **951**, L11 (2023).
[59] L. Mayer, Classical Quantum Gravity **30**, 244008 (2013).
[60] G. Foreman, M. Volonteri, and M. Dotti, Astrophys. J. **693**, 1554 (2009).
[61] M. C. Begelman, R. D. Blandford, and M. J. Rees, Nature (London) **287**, 307 (1980).
[62] E. S. Phinney, arXiv:astro-ph/0108028.
[63] J. Ellis, M. Fairbairn, G. Hütsi, M. Raidal, J. Urrutia, V. Vaskonen, and H. Veermäe, Astron. Astrophys. **676**, A38 (2023).
[64] W. H. Press and P. Schechter, Astrophys. J. **187**, 425 (1974).

[65] J. R. Bond, S. Cole, G. Efstathiou, and N. Kaiser, Astrophys. J. **379**, 440 (1991).
[66] C. G. Lacey and S. Cole, Mon. Not. R. Astron. Soc. **262**, 627 (1993).
[67] J. Kormendy and L. C. Ho, Annu. Rev. Astron. Astrophys. **51**, 511 (2013).
[68] A. E. Reines and M. Volonteri, Astrophys. J. **813**, 82 (2015).
[69] G. Girelli, L. Pozzetti, M. Bolzonella, C. Giocoli, F. Marulli, and M. Baldi, Astron. Astrophys. **634**, A135 (2020).
[70] See Supplemental Material at http://link.aps.org/supplemental/10.1103/PhysRevD.109.L021302 for further discussion on the implications of different scaling relations as well as a more developed mathematical formalism of the computation of the background, which includes Refs. [71–77].
[71] Y. Harikane *et al.*, arXiv:2303.11946.
[72] D. D. Kocevski *et al.*, Astrophys. J. Lett. **954**, L4 (2023).
[73] R. Maiolino *et al.*, arXiv:2308.01230.
[74] F. Pacucci, B. Nguyen, S. Carniani, R. Maiolino, and X. Fan, Astrophys. J. Lett. **957**, L3 (2023).
[75] R. Aversa, A. Lapi, G. de Zotti, F. Shankar, and L. Danese, Astrophys. J. **810**, 74 (2015).
[76] I. Delvecchio *et al.*, Astrophys. J. **892**, 17 (2020).
[77] T. Di Matteo, D. Angles-Alcazar, and F. Shankar, arXiv:2304.11541.
[78] J. Antoniadis *et al.* (EPTA Collaboration), arXiv:2306.16227.
[79] M. Enoki and M. Nagashima, Prog. Theor. Phys. **117**, 241 (2007).
[80] L. Z. Kelley, L. Blecha, L. Hernquist, A. Sesana, and S. R. Taylor, Mon. Not. R. Astron. Soc. **471**, 4508 (2017).
[81] D. Merritt, Classical Quantum Gravity **30**, 244005 (2013).
[82] P. J. Armitage and P. Natarajan, Astrophys. J. Lett. **567**, L9 (2002).
[83] A. I. Macfadyen and M. Milosavljevic, Astrophys. J. **672**, 83 (2008).
[84] Y. Tang, A. MacFadyen, and Z. Haiman, Mon. Not. R. Astron. Soc. **469**, 4258 (2017).
[85] D. J. Muñoz, R. Miranda, and D. Lai, Astrophys. J. **871**, 84 (2019).
[86] M. S. L. Moody, J.-M. Shi, and J. M. Stone, Astrophys. J. **875**, 66 (2019).
[87] C. Tiede, J. Zrake, A. MacFadyen, and Z. Haiman, Astrophys. J. **900**, 43 (2020).
[88] D. J. D'Orazio and P. C. Duffell, Astrophys. J. Lett. **914**, L21 (2021).
[89] P. C. Duffell, D. D'Orazio, A. Derdzinski, Z. Haiman, A. MacFadyen, A. L. Rosen, and J. Zrake, Astrophys. J. **901**, 25 (2020).
[90] Z. Haiman, Z. Haiman, B. Kocsis, B. Kocsis, K. Menou, and K. Menou, Astrophys. J. **700**, 1952 (2009); **937**, 129 (E) (2022).
[91] A. Sesana, Classical Quantum Gravity **30**, 224014 (2013).
[92] L. Z. Kelley, L. Blecha, and L. Hernquist, Mon. Not. R. Astron. Soc. **464**, 3131 (2017).
[93] M. M. Kozhikkal, S. Chen, G. Theureau, M. Habouzit, and A. Sesana, arXiv:2305.18293.
[94] G. Agazie *et al.* (NANOGrav Collaboration), Astrophys. J. Lett. **951**, L50 (2023).
[95] E. A. Huerta, S. T. McWilliams, J. R. Gair, and S. R. Taylor, Phys. Rev. D **92**, 063010 (2015).
[96] J. Antoniadis *et al.* (EPTA Collaboration), arXiv:2306.16226.
[97] P. Amaro-Seoane *et al.* (LISA Collaboration), arXiv:1702.00786.
[98] L. Badurina *et al.* (AION Collaboration), J. Cosmol. Astropart. Phys. 05 (2020) 011.
[99] Y. A. El-Neaj *et al.* (AEDGE Collaboration), Eur. Phys. J. Quantum Technol. **7**, 6 (2020).
[100] V. Corbin and N. J. Cornish, Classical Quantum Gravity **23**, 2435 (2006).
[101] T. Nakamura *et al.*, Prog. Theor. Exp. Phys. **2016**, 093E01 (2016).